Structural Engineering and Mechanics, Vol. 5, No. 6 (1997) 715-728
DOI: http://dx.doi.org/10.12989/sem.1997.5.6.715

Secondary buckling analysis of spherical caps

Shiro Kato†

Department of Architecture and Civil Engineering, Toyohashi University of Technology, Aichi 441, Japan

Yoshinao Chiba‡

Department of Architecture, College of Engineering, Hosei University, Tokyo 184, Japan

Itaru Mutoh‡†

Department of Architecture, Gifu National College of Technology, Gifu 501-04, Japan

Abstract. The aim of this paper is to investigate the secondary buckling behaviour and mode-coupling of spherical caps under uniformly external pressure. The analysis makes use of a rotational finite shell element on the basis of strain-displacement relations according to Koiter's shell theory (Small Finite Deflections). The post-buckling behaviours after a bifurcation point are analyzed precisely by considering multi-mode coupling between several higher order harmonic wave numbers, and on the way of post-buckling path the positive definiteness of incremental stiffness matrix of uncoupled modes is examined step by step. The secondary buckling point that has zero eigen-value of incremental stiffness matrix and the corresponding secondary mode are obtained, moreover, the secondary post-buckling path is traced.

Key words: small finite deflection theory; secondary buckling; mode coupling.

1. Introduction

Koiter was the first to develop an asymptotic theory for initial post-buckling behaviour of perfect and imperfect shell structures. The theory provides the most rational explanation of the large discrepancy between test and theory (Bushnell 1985). There are many papers that handled the post-buckling behaviours with initial imperfection sensitivities, but few papers are available on the secondary-bifurcation points with higher equilibrium paths of shell structures (Krätzig, *et al.* 1982).

In this study the post-buckling and secondary buckling analysis of spherical caps under uniformly external pressure is performed by a well-established computer program (Chiba, *et al.* 1993, Kato, *et al.* 1996) using a rotational finite shell element on the basis of Koiter's Small Finite Deflections shell theory. With sufficient wave numbers for higher harmonic displacement fields, the post-buckling behaviours after bifurcation point are analyzed precisely. On the way of post-

† Professor
‡ Research Associate
‡† Associate Professor

buckling path the positive definiteness of incremental stiffness matrix of uncoupled modes is examined step by step to find the secondary buckling point that has zero eigen-value of incremental stiffness matrix and its corresponding secondary buckling mode is calculated once the zero eigen-value is found. Moreover, the secondary post-buckling path after the secondary buckling point is also traced, and the growth of deformations in several interacting modes is investigated. Besides, with the obtained displacement fields, the total potential energy, strain energy including membrane and bending energy components and Astatic buckling loads are also calculated. From the above energy components, the complicated post-buckling behaviours are investigated minutely.

2. Fundamental assumptions and definition of strains (Chiba, *et al.* 1993)

The rotational shell in this study is shown in Fig. 1, where the reference surface is defined by the coordinate system s and θ. With the deformation of the shell, the following assumptions are made.

1) The shell is thin, and the Kirchhoff-Love hypothesis is enforced.

2) The strains are small, and the geometric nonlinearity is defined as a set of middle surface strains.

3) The shell can be assumed to be an isotropic elastic body.

The strain-displacement relations, according to Koiter's Small Finite Deflections shell theory (Koiter 1966) are expressed in tensor notation as follows.

$$\varepsilon_{ij}=\theta_{ij}+\frac{1}{2}g^{kl}(\theta_{ki}-\omega_{ki})(\theta_{lj}-\omega_{lj})+\frac{1}{2}\varphi_i\varphi_j \quad \text{:In-plane strains} \tag{1}$$

$$\kappa_{ij}=\frac{1}{2}(\varphi_i|_j+\varphi_j|_i)+H_i^l\omega_{jl}+H_j^l\omega_{il} \quad \text{:Bending strains} \tag{2}$$

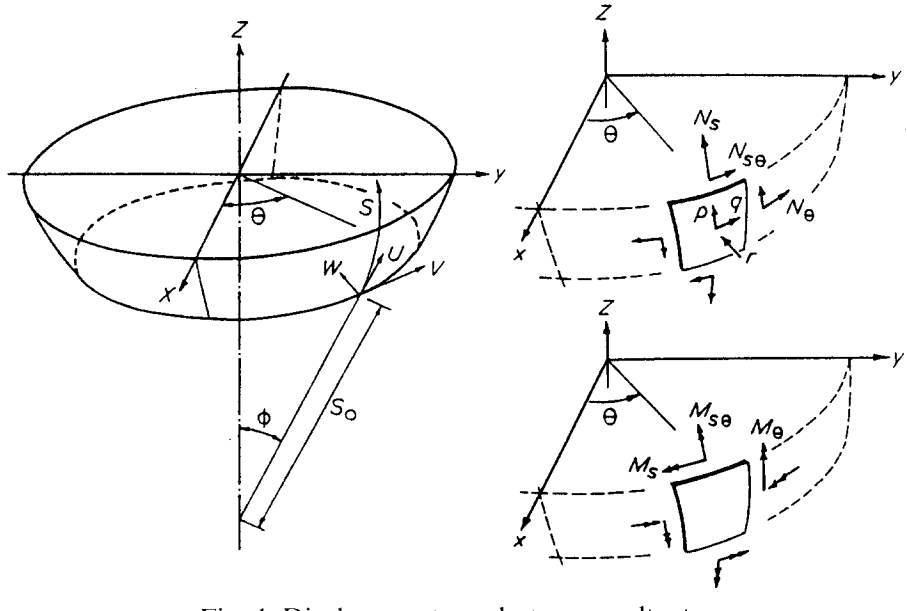

Fig. 1 Displacements and stress resultants.

$$\theta_{ij}=\frac{1}{2}(u_i|_j+u_j|_i)-H_{ij}\omega \qquad \text{:Linearized in-plane strains}$$

$$\omega_{ij}=\frac{1}{2}(u_j|_i-u_i|_j) \qquad \text{:Rotation tensors}$$

$$\varphi_i=\omega_{,i}+H_i^j u_j \qquad \text{:Rotation vectors}$$

where g_{kl} and H_{ij} are the first and second fundamental metric tensors, respectively.

The strain-displacement relations in physical components are expressed as follows:

In-plane strains:

$$\begin{Bmatrix}\varepsilon_{ss}\\ \varepsilon_{\theta\theta}\\ \varepsilon_{s\theta}\end{Bmatrix}=L_m(D)+\frac{1}{2}N_m(D)$$
$$=\begin{Bmatrix}{}_L\varepsilon_s\\ {}_L\varepsilon_\theta\\ {}_L\varepsilon_{s\theta}\end{Bmatrix}+\frac{1}{2}\begin{Bmatrix}{}_L\varepsilon_s{}^2+\phi_s{}^2+V_s{}^2\\ {}_L\varepsilon_\theta{}^2+\phi_\theta{}^2+U_\theta{}^2\\ {}_L\varepsilon_s U_\theta+{}_L\varepsilon_\theta V_s+\phi_s\phi_\theta\end{Bmatrix} \tag{3}$$

Linear in-plane strains:

$$\begin{aligned}
&{}_L\varepsilon_s=\frac{\partial u}{\partial s}+\frac{\partial\varphi}{\partial s}w\\
&{}_L\varepsilon_\theta=\frac{1}{s_0\sin\varphi}\frac{\partial v}{\partial\theta}+\frac{1}{s_0}u-\frac{1}{s_0\tan\varphi}w\\
&{}_L\varepsilon_{s\theta}=\frac{1}{2}\left(\frac{1}{s_0\sin\varphi}\frac{\partial u}{\partial\theta}-\frac{1}{s_0}v+\frac{\partial v}{\partial s}\right)=\frac{1}{2}(U_\theta+V_s)\\
&\phi_s=\frac{\partial w}{\partial s}-\frac{\partial\varphi}{\partial s}u \qquad V_s=\frac{\partial v}{\partial s}\\
&\phi_\theta=\frac{1}{s_0\sin\varphi}\left(\frac{\partial w}{\partial\theta}+\cos\varphi\cdot v\right) \qquad U_\theta=\frac{1}{s_0\sin\varphi}\frac{\partial u}{\partial\theta}-\frac{1}{s_0}v
\end{aligned} \tag{4}$$

Linear bending strains:

$$\begin{aligned}
&\kappa_{ss}=\frac{\partial^2 w}{\partial s^2}-\frac{\partial\varphi}{\partial s}\frac{\partial u}{\partial s}-\frac{\partial^2\varphi}{\partial s^2}u\\
&\kappa_{\theta\theta}=\frac{1}{s_0{}^2\sin^2\varphi}\frac{\partial^2 w}{\partial\theta^2}+\frac{\cos\varphi}{s_0{}^2\sin^2\varphi}\frac{\partial v}{\partial\theta}+\frac{1}{s_0}\left(\frac{\partial w}{\partial s}-\frac{\partial\varphi}{\partial s}u\right)\\
&\kappa_{s\theta}=\frac{1}{s_0\sin\varphi}\frac{\partial^2 w}{\partial s\partial\theta}+\frac{1}{s_0\sin\varphi}\left(-\frac{3}{4}\frac{\partial\varphi}{\partial s}-\frac{1}{4}\frac{1}{s_0\tan\varphi}\right)\frac{\partial u}{\partial\theta}+\\
&\left(\frac{3}{4}\frac{1}{s_0\tan\varphi}+\frac{1}{4}\frac{\partial\varphi}{\partial s}\right)\frac{\partial v}{\partial s}-\frac{1}{s_0{}^2\sin\varphi}\frac{\partial w}{\partial\theta}+\left(-\frac{3}{4}\frac{1}{s_0{}^2\tan\varphi}-\frac{1}{4}\frac{1}{s_0}\frac{\partial\varphi}{\partial s}\right)v
\end{aligned} \tag{5}$$

The geometry of spherical cap and analytical conditions are shown in Fig. 2 and Table 1, respectively. Geometric depth parameter λ of spherical caps is defined as follows:

$$\lambda=2\sqrt[4]{3(1-\nu^2)}\times\sqrt{H/t} \tag{6}$$

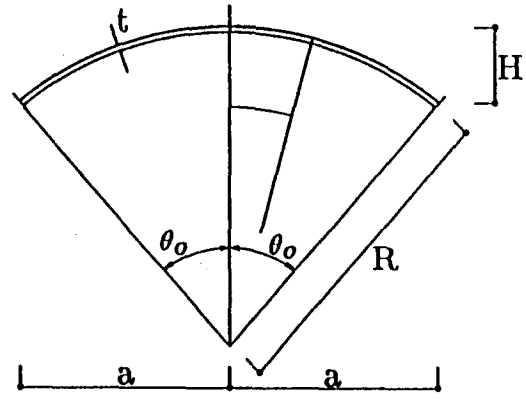

Fig. 2 Geometry of a rotational shell.

Table 1 Analytical condition

Radius	$R=50$cm
Semi-angle	$\theta_0=10°$
Rise	$H=0.75962$cm
Shell thickness	$t=0.13945$cm ($\lambda=6$)
	$t=0.10246$cm ($\lambda=7$)
	$t=0.07804$cm ($\lambda=8$)
Young's modulus	$E=206$GPa
Poisson's ratio	$\nu=0.3$
Boundary condition	Clamed edge
Loading condition	External pressure ($n=0$)

3. Numerical method (Kato, *et al.* 1996)

In the case of a rotational shell element, the displacement components u, v and w are described by Fourier series as follows:

$$\begin{Bmatrix} u \\ v \\ w \end{Bmatrix} = \sum_{n=0}^{m} \begin{Bmatrix} u_n(s)\cos n\theta \\ v_n(s)\sin n\theta \\ w_n(s)\cos n\theta \end{Bmatrix} \tag{7}$$

where n is the harmonic wave number and $u_n(s)$, $v_n(s)$, $w_n(s)$ are displacement interpolation functions in the direction of arc length s in harmonic n, by the Hermitian cubic shape function.

According to the usual FE method for geometrically nonlinear problems, the governing equation for the rotational shell is obtained from the stationary condition of the total potential energy. Incremental equilibrium equation is as follows:

$$([\boldsymbol{K}_{LM}]+[\boldsymbol{K}_{U}]+[\boldsymbol{K}_{\sigma}]+[\boldsymbol{K}_{LB}])\{\boldsymbol{\Delta D}\}=\{\boldsymbol{Q}_{e}\}+\{\boldsymbol{\Delta Q}_{e}\}-\{\boldsymbol{Q}_{iM}\}-\{\boldsymbol{Q}_{iB}\} \tag{8}$$

or in another expression,

$$[\boldsymbol{K}_{incr}]\{\Delta\boldsymbol{D}\}=\{\Delta\boldsymbol{P}\}$$

$[\boldsymbol{K}_{LM}]$, $[\boldsymbol{K}_{LB}]$: Linear in-plane and bending stiffness matrix
$[\boldsymbol{K}_{U}]$: Initial displacement matrix
$[\boldsymbol{K}_{\sigma}]$: Initial stress stiffness matrix
$\{\Delta\boldsymbol{D}\}$: Incremental displacement vector
$\{\boldsymbol{Q}_{e}\}$, $\{\Delta\boldsymbol{Q}_{e}\}$: External load and incremental load vector
$\{\boldsymbol{Q}_{iM}\}$, $\{\boldsymbol{Q}_{iB}\}$: In-plane and bending internal load vector

In this study the integral of stiffness matrix with respect to arc length (s) is carried out by Newton-Cotes 6-point numerical integration scheme, and the integral with respect to Fourier expansions (θ) can be evaluated analytically according to the following equations. Mode coupling between $n=i\theta$ and $n=j\theta$ can be examined easily.

$$\begin{aligned}
CC(I,J)&=\int_0^{2\pi}\cos i\theta\cos j\theta d\theta\\
SS(I,J)&=\int_0^{2\pi}\sin i\theta\sin j\theta d\theta\\
CCC(I,J,K)&=\int_0^{2\pi}\cos i\theta\cos j\theta\cos k\theta d\theta\\
CSS(I,J,K)&=\int_0^{2\pi}\cos i\theta\sin j\theta\sin k\theta d\theta\\
CCCC(I,J,K,L)&=\int_0^{2\pi}\cos i\theta\cos j\theta\cos k\theta\cos l\theta d\theta\\
SSSS(I,J,K,L)&=\int_0^{2\pi}\sin i\theta\sin j\theta\sin k\theta\sin l\theta d\theta\\
CSCS(I,J,K,L)&=\int_0^{2\pi}\cos i\theta\sin j\theta\cos k\theta\sin l\theta d\theta
\end{aligned}\tag{9}$$

In case of axisymmetric loading, the incremental equilibrium equation on the fundamental path (yielding only axisymmetric prebuckling deformation) is:

$$\begin{Bmatrix}
\boldsymbol{K}_{00} & 0 & 0 & 0 & 0 & 0\\
 & \boldsymbol{K}_{11} & 0 & 0 & 0 & 0\\
 & & \boldsymbol{K}_{22} & 0 & 0 & 0\\
 & & & \boldsymbol{K}_{33} & 0 & 0\\
 & & & & \boldsymbol{K}_{44} & 0\\
 & & \text{symm.} & & & \boldsymbol{K}_{55}
\end{Bmatrix}
\begin{Bmatrix}\Delta d_0\\ \Delta d_1\\ \Delta d_2\\ \Delta d_3\\ \Delta d_4\\ \Delta d_5\end{Bmatrix}=
\begin{Bmatrix}\Delta P_0\neq 0\\ \Delta P_1=0\\ \Delta P_2=0\\ \Delta P_3=0\\ \Delta P_4=0\\ \Delta P_5=0\end{Bmatrix}\tag{10}$$

where ($\boldsymbol{K}_{nn}$, $n=0, 1, 2, 3, 4, 5$) are the incremental stiffness matrices with respect to Fourier expansion n (harmonic wave number), that are not coupled with other harmonics on the fundamental equilibrium path.

To search the asymmetric bifurcation loads, the eigen-value of the incremental stiffness matrix (tangential matrix) in asymmetric harmonic wave number ($n \neq 0$) is checked throughout the loading step. If zero eigen-value (or negative definite) is found, the eigen-vector is to be searched as the asymmetric bifurcation mode.

In this study, in order to evaluate the higher order terms due to modal coupling, deformations after a bifurcation point are represented with four Fourier terms. For example, in case of bifurcation mode n_{cr}, deformation modes $n=0$, $n=n_{cr}$, $n=2n_{cr}$, $n=3n_{cr}$ (after this, denoting by $n=0+n_{cr}+2n_{cr}+3n_{cr}$) are used for the superposition of deformations. From the bifurcation point, the adjacent post-buckling path can be searched by using displacement incremental method with the acquired asymmetric bifurcation mode.

For example, in case of bifurcation mode $n_{cr}=3$, the incremental equilibrium equation on the post-buckling path is:

$$\begin{Bmatrix} K_{00} & K_{03} & K_{06} & K_{09} \\ & K_{33} & K_{36} & K_{39} \\ & & K_{66} & K_{69} \\ & \textit{symm.} & & K_{99} \end{Bmatrix} \begin{Bmatrix} \Delta d_0 \\ \Delta d_3 \\ \Delta d_6 \\ \Delta d_7 \end{Bmatrix} = \begin{Bmatrix} \Delta P_0 \neq 0 \\ \Delta P_3 = 0 \\ \Delta P_6 = 0 \\ \Delta P_9 = 0 \end{Bmatrix} \tag{11}$$

Furthermore, on the post-buckling path, the eigen-value of stiffness matrix for uncoupled harmonic wave numbers is checked just like as post-buckling mode searching. Let us consider the post-buckling mode of $n_{cr}=3$. On this case the post-buckling deformation is described by the superposition of harmonic wave numbers ($n=0+3+6+9$), and the secondary buckling mode is determined by ($n=1+2+4+5$). Then, the secondary post-buckling path is described by ($n=0+3+6+9+1+2+4+5$). The schematic representations of the coupled and uncoupled incremental stiffness matrix are shown as follows.

The incremental equilibrium equation after bifurcation is:

$n=0+3+6+9$: post-buckling deformation modes after bifurcation
$n=1+2+4+5$: secondary buckling modes

$$\begin{Bmatrix} K_{00} & 0 & 0 & K_{03} & 0 & 0 & K_{06} & K_{09} \\ & K_{11} & K_{12} & 0 & K_{14} & K_{15} & 0 & 0 \\ & & K_{22} & 0 & K_{24} & K_{25} & 0 & 0 \\ & & & K_{33} & 0 & 0 & K_{36} & K_{39} \\ & & & & K_{44} & K_{45} & 0 & 0 \\ & & & & & K_{55} & 0 & 0 \\ & & \text{symm.} & & & & K_{66} & K_{69} \\ & & & & & & & K_{99} \end{Bmatrix} \begin{Bmatrix} \Delta d_0 \\ \Delta d_1 \\ \Delta d_2 \\ \Delta d_3 \\ \Delta d_4 \\ \Delta d_5 \\ \Delta d_6 \\ \Delta d_9 \end{Bmatrix} = \begin{Bmatrix} \Delta P_0 \neq 0 \\ \Delta P_1 = 0 \\ \Delta P_2 = 0 \\ \Delta P_3 = 0 \\ \Delta P_4 = 0 \\ \Delta P_5 = 0 \\ \Delta P_6 = 0 \\ \Delta P_9 = 0 \end{Bmatrix}$$

Rearranging rows and columns of the above equation,

$$\begin{Bmatrix} K_{00} & K_{03} & K_{06} & K_{09} & 0 & 0 & 0 & 0 \\ & K_{33} & K_{36} & K_{39} & 0 & 0 & 0 & 0 \\ & & K_{66} & K_{69} & 0 & 0 & 0 & 0 \\ & & & K_{99} & 0 & 0 & 0 & 0 \\ & & & & K_{11} & K_{12} & K_{14} & K_{15} \\ & & & & & K_{22} & K_{24} & K_{25} \\ & & \text{symm.} & & & & K_{44} & K_{45} \\ & & & & & & & K_{55} \end{Bmatrix} \begin{Bmatrix} \Delta d_0 \\ \Delta d_3 \\ \Delta d_6 \\ \Delta d_9 \\ \Delta d_1 \\ \Delta d_2 \\ \Delta d_4 \\ \Delta d_5 \end{Bmatrix} = \begin{Bmatrix} \Delta P_0 \neq 0 \\ \Delta P_3 \\ \Delta P_6 \\ \Delta P_9 \\ \Delta P_1 = 0 \\ \Delta P_2 = 0 \\ \Delta P_4 = 0 \\ \Delta P_5 = 0 \end{Bmatrix} \tag{12}$$

All components, ΔP_1, ΔP_2, ΔP_4 and ΔP_5, of the secondary buckling modes ($n=1+2+4+5$) are zero on the way of post-buckling path because of uncoupling between ($n=0+3+6+9$) and ($n=1+2+4+5$).

On the way of post-buckling path, the following eigen-value (μ) of the uncoupled incremental stiffness matrix ($n=1+2+4+5$) is examined step by step as stated above, and the load that sign of μ is to be changed from positive to negative just at the secondary buckling can be obtained exactly by half-interval search method.

$$\begin{Bmatrix} K_{11} & K_{12} & K_{14} & K_{15} \\ & K_{22} & K_{24} & K_{25} \\ & & K_{44} & K_{45} \\ & \text{symm.} & & K_{55} \end{Bmatrix} \begin{Bmatrix} \Delta d_1 \\ \Delta d_2 \\ \Delta d_4 \\ \Delta d_5 \end{Bmatrix} = \mu \begin{Bmatrix} \Delta d_1 \\ \Delta d_2 \\ \Delta d_4 \\ \Delta d_5 \end{Bmatrix} \tag{13}$$

The incremental equilibrium equation after secondary buckling is:

$$\begin{Bmatrix} K_{00} & K_{01} & K_{02} & K_{03} & K_{04} & K_{05} & K_{06} & K_{09} \\ & K_{11} & K_{12} & K_{13} & K_{14} & K_{15} & K_{16} & K_{19} \\ & & K_{22} & K_{23} & K_{24} & K_{25} & K_{26} & K_{29} \\ & & & K_{33} & K_{34} & K_{35} & K_{36} & K_{39} \\ & & & & K_{44} & K_{45} & K_{46} & K_{49} \\ & & & & & K_{55} & K_{56} & K_{59} \\ & & \textit{symm.} & & & & K_{66} & K_{69} \\ & & & & & & & K_{99} \end{Bmatrix} \begin{Bmatrix} \Delta d_0 \\ \Delta d_1 \\ \Delta d_2 \\ \Delta d_3 \\ \Delta d_4 \\ \Delta d_5 \\ \Delta d_6 \\ \Delta d_9 \end{Bmatrix} = \begin{Bmatrix} \Delta P_0 \neq 0 \\ \Delta P_1 \\ \Delta P_2 \\ \Delta P_3 \\ \Delta P_4 \\ \Delta P_5 \\ \Delta P_6 \\ \Delta P_9 \end{Bmatrix} \tag{14}$$

All components of deformation modes are coupling each other after secondary buckling.

4. Computations for analysis

To solve the nonlinear incremental equilibrium equations, the Newton-Raphson scheme and modified Riks-Wempner method (Ramm 1982, Crisfield 1991) are used together with FE discretization. Each model is discretized by 24 rotational elements with 25 nodes, and each node has 6 D.O.F. Therefore the number of D.O.F. for each circumferential mode sums up to 95 for $n=0$ (axisymmetric mode, $\Delta \boldsymbol{d}_0$ in Eq. (14)), 145 for $n=1$ ($\Delta \boldsymbol{d}_1$ in Eq. (14)) and 142 for $n\geq 2$ (for example, $\Delta \boldsymbol{d}_2$ in Eq. (14)), respectively. In case of post-secondary buckling analysis, symmetric full matrix with 1092 D.O.F. must be reformed by numerical integration in every load step and each iteration. In this study, the integral calculations of total potential and strain energy associated with actual deformations are carried out at each equilibrium state using Newton-Cotes 6-point numerical integration scheme just like as the linear and nonlinear stiffness matrix. All numerical calculations were performed by using VPX210/10 vectorized supercomputer (Memory 256MB, nominal CPU speed 625MFlops) at Hosei University.

5. Asymmetric bifurcation loads and post-buckling behaviours

The results of the asymmetric bifurcation buckling load (P_{cl}^{bf}) are shown in Table 2, and the values in the parentheses are the results of Huang's reliable bifurcation loads (Huang 1964).

Table 2 Asymmetric bifurcation buckling load P_{cl}^{bf}/P_{cl}

	$\lambda=6$	$\lambda=7$	$\lambda=8$
$n=0$	0.971 (0.995)	1.045 (1.068)	1.107 (1.130)
$n=1$	0.906 (0.919)	–	–
$n=2$	0.763 (0.775)	0.784 (0.796)	0.880 (0.893)
$n=3$	0.817 (0.827)	0.750 (0.760)	0.764 (0.774)
$n=4$	–	0.803 (0.812)	0.758 (0.766)
$n=5$	–	–	0.805 (0.813)

where $P_{cl}=2E/\sqrt{3(1-\nu^2)}\cdot(t/R)^2$: classical buckling load

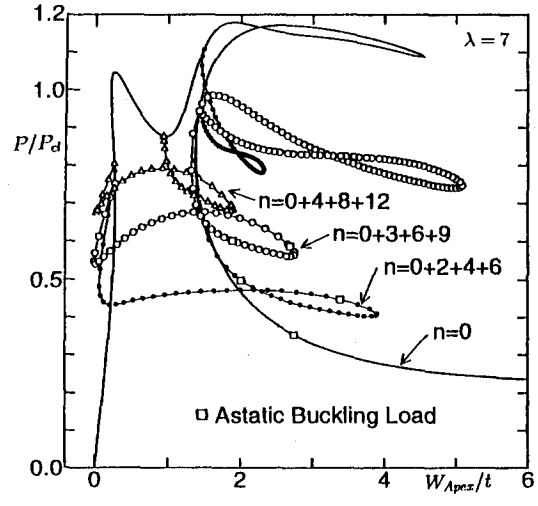

Fig. 3 Load-deflection curve ($\lambda=7$).

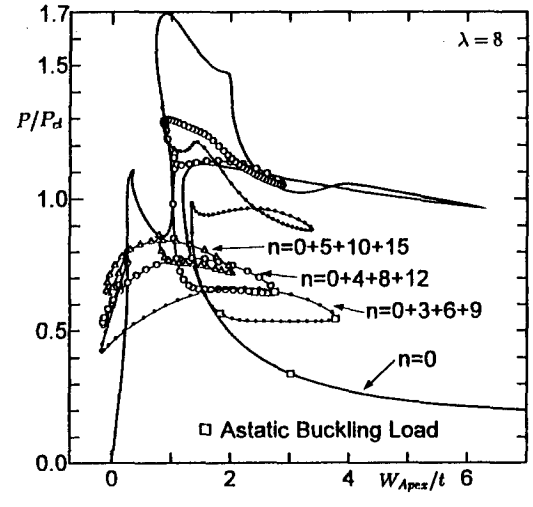

Fig. 4 Load-deflection curve ($\lambda=8$).

For $\lambda=7$ and $\lambda=8$, the post-buckling behaviours with buckling mode $n_{cr}=2$, 3, 4 and 5 could be traced as shown in Fig. 3 and 4. The paths that are rising and falling complicatedly after bifurcation points, and on the way of post-buckling paths, non-axisymmetric components disappear finally. These results are calculated precisely by considering multi-mode coupling with several higher order harmonic wave numbers, but no previous paper could be compared for the buckling analyses of spherical caps.

6. Secondary buckling loads and behaviours

For $\lambda=6$, the secondary buckling point that has zero eigen-value of uncoupled incremental stiffness matrix ($n=1+3+5+7$) could be found just right after the bifurcation point on the

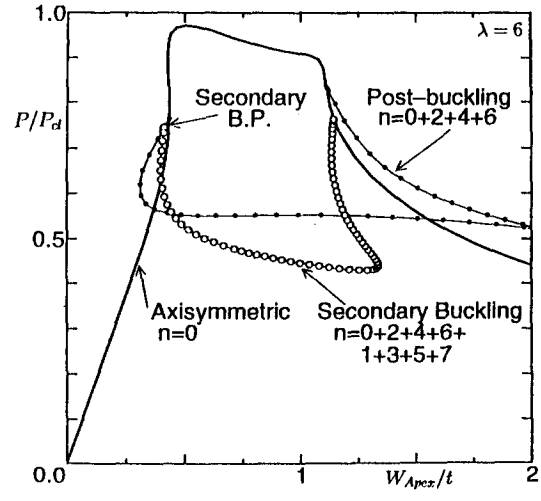

Fig. 5 Load-deflection curve ($\lambda=6$).

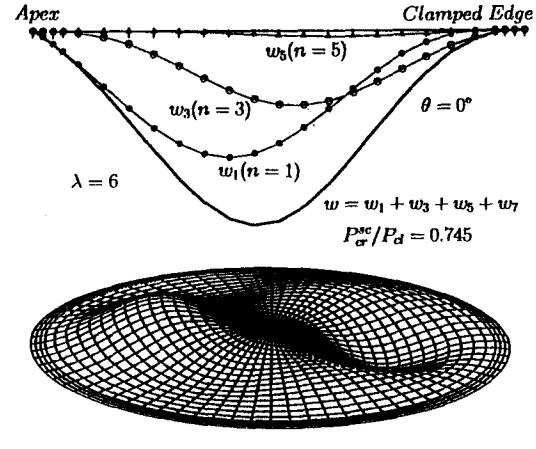

Fig. 6 Secondary buckling mode ($\lambda=6$).

way of post-buckling path ($n=0+2+4+6$) as shown in Fig. 5, and the associated secondary buckling mode determined by ($n=1+3+5+7$) is shown in Fig. 6. Similarly, the load-deflection curve and secondary buckling mode ($n=1+2+4+5$) for $\lambda=7$ are shown in Figs. 7 and 8. The secondary post-buckling behaviours (after secondary bifurcation) could be traced as shown in Figs. 5 and 7, and the load falls gently but decreases considerably in comparison with the post-buckling after the first bifurcation.

The secondary buckling modes are shown in Figs. 6 and 8. In comparison of the bifurcation mode n_{cr} on the axisymmetric prebuckling path, the secondary mode on the post-buckling path has several harmonic wave numbers and the mode of harmonic number ($n_{cr}-1$) is predominant. These tendencies are common to every case for λ, and it indicates that the complicated mode coupling occurs near the secondary buckling points.

The results of the secondary buckling loads are shown in Table 3.

As shown in this table, the bifurcation points and secondary buckling points are adjacent

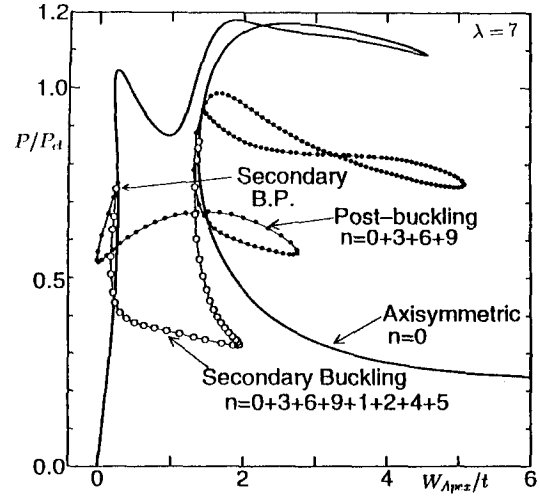

Fig. 7 Load-deflection curve ($\lambda=7$).

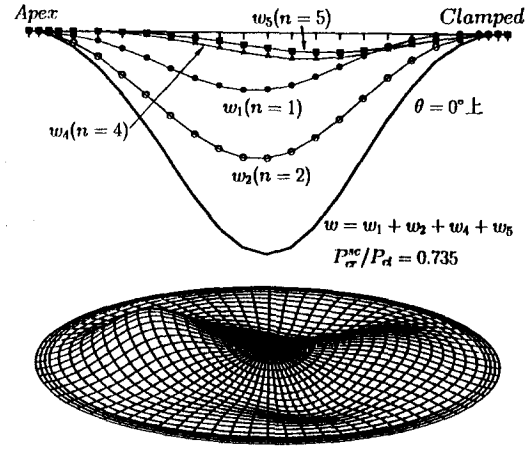

Fig. 8 Secondary buckling mode ($\lambda=7$).

Table 3 Secondary buckling load P_{cr}^{sc}/P_{cl}

λ	wave numbers for post-buckling path	wave numbers for secondary buckling	P_{bf}^{el}/P_{cl} bifurcation load	P_{cr}^{sc}/P_{cl}
6	$n=0+2+4+6$	$n=1+3+5+7$	0.763 ($n=2$)	0.745
7	$n=0+3+6+9$	$n=1+2+4+5$	0.750 ($n=3$)	0.735
8	$n=0+4+8+12$	$n=2+6+10+14$	0.758 ($n=4$)	0.732
8	$n=0+4+8+12$	$n=1+3+5+7$	0.758 ($n=4$)	0.753

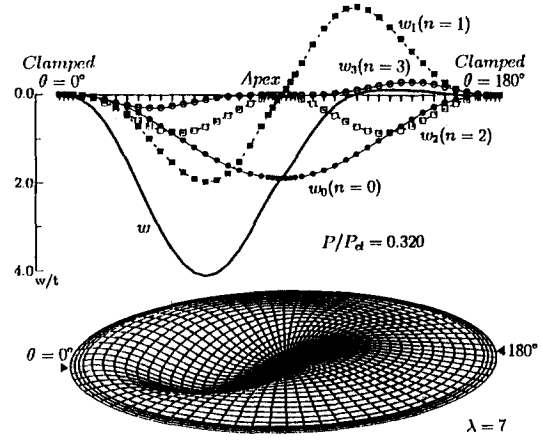

Fig. 9 Deformation mode ($\lambda=7$).

to each other, and on the way of post-buckling path re-bifurcation occurs by appearing lower harmonic wave number than the first bifurcation one. Generally speaking, the collapse pressure of imperfect spherical caps depend on the shapes of the imperfections. Since a general imperfection will contain harmonics of several modes, it seems that mode coupling has an important role in sensitivity problems of load carrying capacity to initial imperfections.

7. Deformation modes after secondary buckling

The deformation mode at the lowest load on the secondary buckling path for $\lambda=7$ is very interesting as shown in Fig. 9, because several harmonic wave numbers ($n=0+3+6+9+1+2+4+5$) are canceling out each other and the deformation is confined to the narrow part of the cap and it appears to form a single narrow dimple. For the case of $\lambda=6$ the same deformation mode can be obtained.

The load-deflection curve for $\lambda=8$ is shown in Fig. 10, and the deformations after secondary buckling at the equilibrium states A and B are very different from the case of $\lambda=6$ and 7. Several modes ($n=0+4+8+12+2+6+10+14$) are amplifying each other to the contrary and the deformation spreads over the whole part of the cap, as shown in Fig. 11 and 12, and it appears to form a large dimple and turn over.

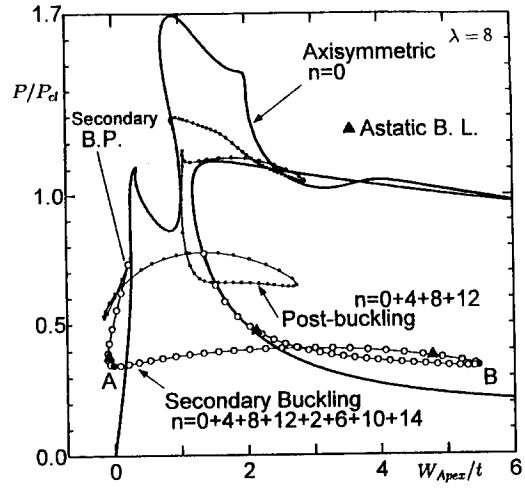

Fig. 10 Load-deflection curve ($\lambda = 8$).

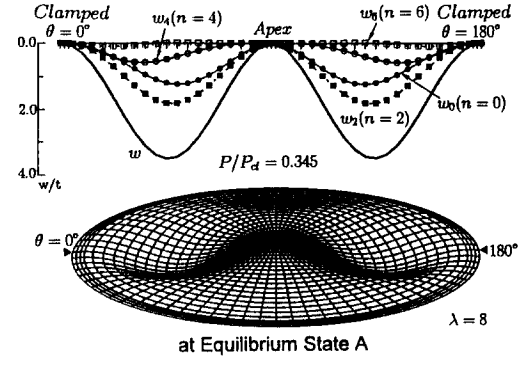

Fig. 11 Deformation mode ($\lambda = 8$).

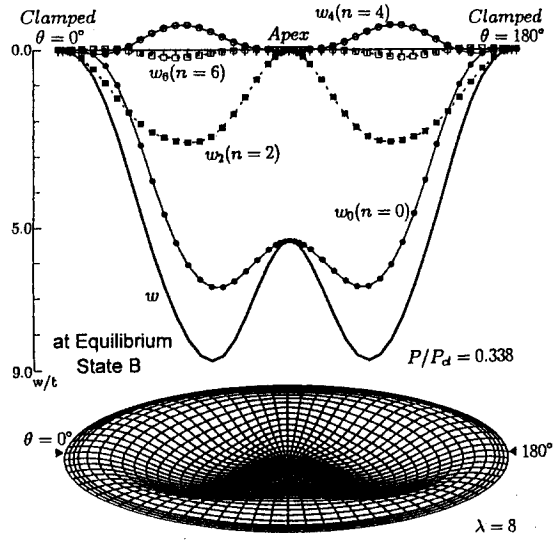

Fig. 12 Deformation mode ($\lambda = 8$).

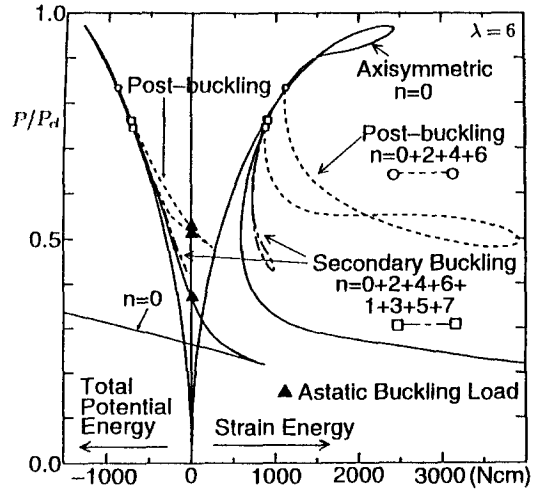

Fig. 13 Load-energy curve ($\lambda = 6$).

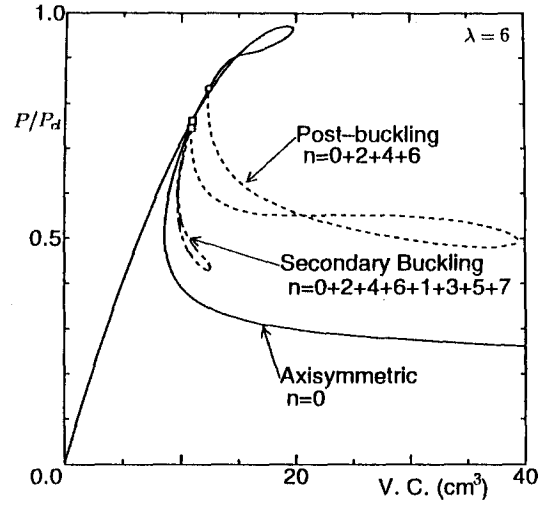

Fig. 14 Load-volume change curve ($\lambda = 6$).

8. Strain energy and volume change

In this study the external potential energy and strain energy associated with actual deformations are calculated at each equilibrium state, and one example of the load-energy curve is shown in Fig. 13. In this figure, Astatic buckling loads for the equilibrium state that has zero total potential energy are also shown. In case of uniformly external pressure, external potential energy can be regarded as the volume change of the deformed cap. This is because only the axisymmetric deformation takes part in volume change.

Making a comparison between the post buckling and secondary post-buckling, volume changes after bifurcation are very different, as shown in Fig. 14. On the post-buckling path, the axisymmetric deformation is very large and spreads over the whole part of the cap. As a result, the volume change of deformation becomes very large. In case of the secondary buckling path for $\lambda = 6$,

non-axisymmeric modes are predominant and volume change of deformation is very small like as the case for deformation mode of $\lambda=7$ in Fig. 9. According to Figs. 13 and 14, on the secondary buckling path it seems that the behaviour of deformation is determined by growing or disappearing of non-axisymmetric components with little change of axisymmetric one.

9. Conclusions

The following several conclusions can be drawn. (a) The secondary buckling point could be found just right after bifurcation point on the way of post-buckling path, and the secondary buckling mode is a very complicated deformation due to mode coupling between several harmonic wave numbers. (b) The higher equilibrium paths and buckling behaviours after secondary buckling could be traced minutely. In comparison with the cases of post-buckling path, the loading capacity is fairly decreased on the way of the secondary post-buckling path. Similarly, there is a difference between the two judging from the view of strain energy change. (c) For $\lambda=6$ and 7, the volume change of deformation mode after secondary buckling is very small and non-axisymmeric modes are noticeable, but the deformation is confined to the narrow part of the cap. (d) For $\lambda=8$, the volume change of deformation mode is very large, and the deformation spreads over the whole part of the cap.

The bifurcation points and secondary buckling points are adjacent to each other, and on the way of post-buckling path re-bifurcation occurs accompanied by appearing lower harmonic wave number than the first bifurcation one. Therefore it seems that mode coupling near the secondary buckling point has an important role in sensitivity problems of load carrying capacity to initial imperfections.

The method used here may be also useful to the secondary buckling problems of other type of shells of revolution, for example, circular cylindrical shells.

References

Bushnell, D. (1985), *Computerized Buckling Analysis of Shells*, Martinus Nijhoff Publishers, Dordrecht, Netherlands.

Krätzig, W.B., Basar, Y. and Wittek, U. (1982), "Nonlinear behaviour and elastic stability of shells-theoretical concepts-numerical computations-results", *Proc. of a State-of-the-Art Colloquium Universitat Stuttgart*, Stuttgart, 19-56.

Chiba, Y., Kato, S. and Mutoh, I. (1993), "Various expressions for elastic buckling loads of spherical caps", *Proc. of the SEIKEN-IASS Symposium*, Tokyo, 129-136.

Koiter, W.T. (1966), "On the nonlinear theory of thin elastic shells", *Proc. Koninkl. Ned. Akad. van Wetenschappen*, Amsterdam, Series B, 69, 1-54.

Kato, S., Mutoh, I. and Chiba, Y. (1996), "Alternative lower bounds analysis of elastic thin shells of revolution", *Engineering Computations, International Journal for Computer-Aided Engineering & Software*, **13**(2/3/4), 41-75.

Ramm, E. (1982), "The riks/wempner approach-an extension of the displacement control method in nonlinear analysis", *Non-linear Computational Mechanics*, ed. by E. Hinton, et al., Pineridge Press, 63-86.

Crisfield, M.A. (1991), *Non-linear Finite Element Analysis of Solids and Structures*, **1**, John Wiley & Sons.

Huang, N.C. (1964), "Unsymmetrical buckling of thin shallow spherical shells", *J. of Appl. Mech. ASME*, **31**, 447-457.

Kato, S., Chiba, Y. and Mutoh, I. (1996), "Secondary buckling analysis of spherical caps", *Proc. of the Third Asian-Pacific Conference on Computational Mechanics (APCOM)*, Seoul, **1**, 485-490.